BEILSTEIN ARCHIVES

This open access document is posted as a preprint in the Beilstein Archives at https://doi.org/10.3762/bxiv.2024.34.v1 and is considered to be an early communication for feedback before peer review. Before citing this document, please check if a final, peer-reviewed version has been published.

This document is not formatted, has not undergone copyediting or typesetting, and may contain errors, unsubstantiated scientific claims or preliminary data.

Preprint Title AFMDAQ Visualizer: Software and guide to reconstruct and analyze images with raw external data acquisition from the atomic force microscopies

Authors David Fernandez Brito, Eduardo Antonio Murillo Bracamontes, Christian Ivan Enriquez Flores and Jose Juan Gervacio Arciniega

Publication Date 03 Juni 2024

Article Type Full Research Paper

Supporting Information File 1 Supporting information.docx; 881.3 KB

ORCID® iDs David Fernandez Brito - https://orcid.org/0009-0002-8347-9901; Christian Ivan Enriquez Flores - https://orcid.org/0000-0002-1110-2905; Jose Juan Gervacio Arciniega - https://orcid.org/0000-0001-7965-4493

License and Terms: This document is copyright 2024 the Author(s); licensee Beilstein-Institut.

This is an open access work under the terms of the Creative Commons Attribution License (https://creativecommons.org/licenses/by/4.0). Please note that the reuse, redistribution and reproduction in particular requires that the author(s) and source are credited and that individual graphics may be subject to special legal provisions.
The license is subject to the Beilstein Archives terms and conditions: https://www.beilstein-archives.org/xiv/terms.
The definitive version of this work can be found at https://doi.org/10.3762/bxiv.2024.34.v1

AFMDAQ Visualizer: Software and guide to reconstruct and analyze images with raw external data acquisition from the atomic force microscopies

David Fernandez Brito[1], Eduardo Antonio Murillo Bracamontes[2*], Christian Ivan Enriquez Flores[3], Jose Juan Gervacio Arciniega[4**]

[1]Facultad de Ciencias Físico Matemáticas, Benemérita Universidad Autónoma de Puebla, Puebla, México

[2]Centro de Nanociencias y Nanotecnología, Universidad Nacional Autónoma de México, Ensenada, México.

[3]TECNM campus Querétaro, Av. Tecnológico s/n esq. Gral. Mariano Escobedo. Colonia Centro Histórico C.P. 76000, Querétaro, Qro.

[4]CONAHCYT-Facultad de Ciencias Físico Matemáticas, Benemérita Universidad Autónoma de Puebla, Puebla, México

*emurillo@ens.cnyn.unam.mx

** jjgervacio@fcfm.buap.mx

Abstract

Atomic force microscopy (AFM) serves as a versatile tool widely employed for the micro- and nanoscale characterization of materials, offering valuable insights into their morphology and physical properties. Despite the proposal of numerous new AFM technologies each year, engineers and researchers encounter a primary challenge in the efficient external acquisition of data and subsequent image reconstruction. Additionally, most AFM users are constrained to analyzing images provided by commercial scanning probe microscopes. However, by acquiring real raw data from the AFM, comprehensive studies of topography and physical

properties become feasible. This paper presents a comprehensive guide to external data capture using data acquisition cards and image reconstruction for topographical and physical properties analysis. Furthermore, open-source programs for data acquisition (AFMDAQ Acquisition) and analysis (AFMDAQ Visualizer) have been developed with a specific focus on advancing external modes in AFM. The discussion encompasses key methodologies and essential tools aimed at enhancing AFM capabilities across diverse research applications.

Keywords: Atomic Force Microscopy, image, Acquisition data card, raw data.

Introduction

Since its inception in 1986 by Gerber and Quate [1], the atomic force microscope (AFM) has emerged as a powerful tool for characterizing the three-dimensional morphology of sample surfaces in both air and liquid environments at micro and nanometer scales. The diverse range of interactions between the AFM tip and the sample enables the detection of various physical properties at these levels, leading to the development of several AFM modalities. Recently, Dokukin and Sokolov introduced the ringing AFM mode, which enhances the capabilities of force-distance modes in probing mechanical properties at the nanoscale [2]. Moreover, multi-frequency surface strain force microscopy [3] has been developed to augment existing modalities such as piezoresponse force microscopy (PFM) [4, 5], atomic force infrared spectroscopy (AFM-IR) or photothermal induced resonance (PTIR) [6–8], piezomagnetic force microscopy (PmFM) [4, 9], atomic force acoustic microscopy (AFAM) [10, 11], and scanning Joule expansion microscopy (SJEM) [12]. In the

development of these new AFM techniques, the acquisition and analysis of external data generated by the AFM are imperative. While software tools for AFM image analysis and reconstruction have been developed, a significant focus has been placed on studying mechanical properties through the analysis of force-distance (F-D) curves, exemplified by the nanite software developed in Python [13]. Additionally, the Python Force Microscopy Laboratory (PyFMLab) software has been designed to determine the viscoelastic properties of samples from conventional F-D curves [14]. The AtomicJ software, developed in Java, analyzes F-D curves to produce maps of mechanical properties [15]. Other software tools, such as TopoStats, have been developed to identify and track specific biomolecules from AFM images [16]. In addition to the AFM software mentioned above, in some works analyzed the AFM data to improve the image resolution [17–19] or to increase the AFM scan speed [20]. The most popular free software packages for AFM image processing, such as Gwyddion [21] and WSxM [22], have limitations in reading and reconstruct only the data generated by the commercial AFM systems. These data are typically pre-processed by the AFM systems, concealing certain pixel-by-pixel information that may be crucial for the ongoing study, as demonstrated in this work. Despite these advancements, challenges persist in accessing, sharing, and comparing AFM data due to the diverse proprietary file formats offered by AFM companies. One potential solution to this issue is the utilization of an external data acquisition system (DAQ), which allows for the retrieval of raw data from the AFM for post-processing and pixel-by-pixel analysis. However, there remains a gap in the literature regarding the detailed reconstruction of AFM topography images and physical properties from raw

data acquired using a DAQ. In this study, we present a methodology for acquiring raw AFM data using a DAQ and demonstrate how to reconstruct topography images and certain physical properties using open source programs developed in Python. This methodology can facilitate the development and adaptation of new microscopy techniques for AFM systems and aid in the comprehension of AFM fundamentals for new users.

Results and discussion

External reconstruction of topography image from AFM in contact mode by using a portable data acquisition card.

For the external implementation and development of new microscopies in an AFM, it is necessary to externally reconstruct the topography of the surface sample and associate certain zones of the sample with its physical properties measured through the implemented or developed microscopy. The AFM generates topography images by scanning lines, which are formed by pixels. Generally, the options for choosing the length of our image are determined by the number of lines, which need to be a multiple of 16. The number of pixels is determined by the square of the number of lines; for example, if the image consists of 256 lines, the number of pixels is 256 x 256 = 65536.

The AFM systems uses frame, line, and pixel reference signals for image reconstruction. The frame denotes the start and end of the scanned image. The line indicates the start and end of each line, while the pixels mark the start and end of

every pixel. In the case of a 16 pixel x 16 pixel configuration, the frame, line, and pixel references are illustrated in Figure 1.

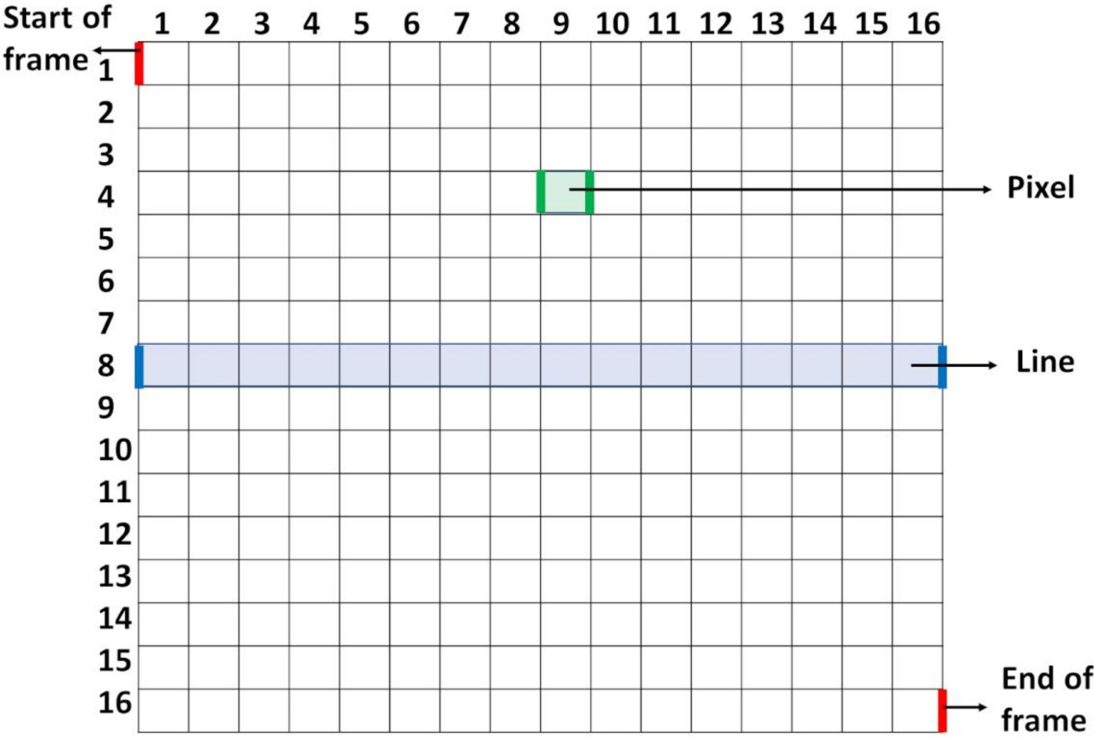

Figure 1. Reference signals frame, line, and pixel used for constructing images in the AFM. The red lines represent the start and end of the frame. The blue lines delineate the beginning and end of line 8. The green lines mark the start and end of the pixel in row 4 and column 9.

The data acquisition for topography reconstruction is performed using a portable NI USB-6356 data acquisition card. This DAQ features eight analog input channels and a maximum sample rate of 1.25 MS/s per channel. The frame, line, and pixel signals (from the SPM Controller) as well as the z signals (from the signal access module) are connected to the DAQ, as depicted in Figure 2.

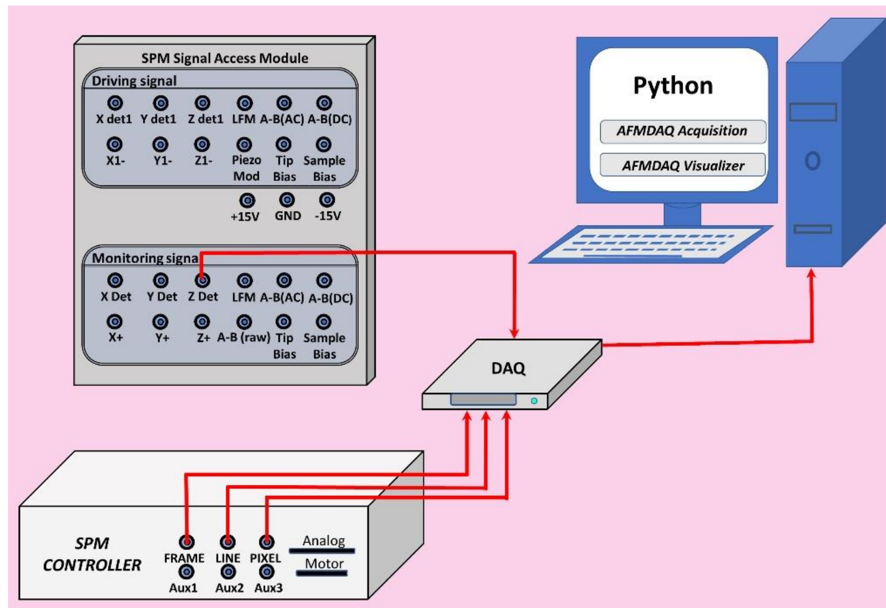

Figure 2. Topography data acquisition set up.

The DAQ is controlled by a Python program; Python program can be downloaded from their respective website (https://www.python.org/), Python has the advantage of being open source and free of charge. The scanning time of the complete image determines the cycles of the DAQ; for example, a scanning time of 9 minutes for an image requires approximately 16,000 cycles using the NI USB-6356. The z, frame, line, and pixel signals can be acquired by the DAQ in real time and generate a comma-separated value (CSV) file with 4 columns corresponding to the z, frame, line, and pixel.

For example, a 64 pixel x 64 pixel image was obtained by scanning the surface of the hard disk in contact mode, with a scan rate of 1 Hz, using an ElectricCont-G cantilever from Budget Sensors, the sample from the hard drive was obtained by cutting it from a broken unit. A CSV file with 4 columns was generated. This file

includes text in the first five rows, as shown in Figure 3a. It is convenient to open the CSV file in a notepad program to remove these text rows and facilitate the subsequent analysis, as illustrated in Figure 3b. In our case, column 0 contains the frame signal, column 1 contains the line signal, column 2 contains the pixel signal, and column 3 contains the z signal.

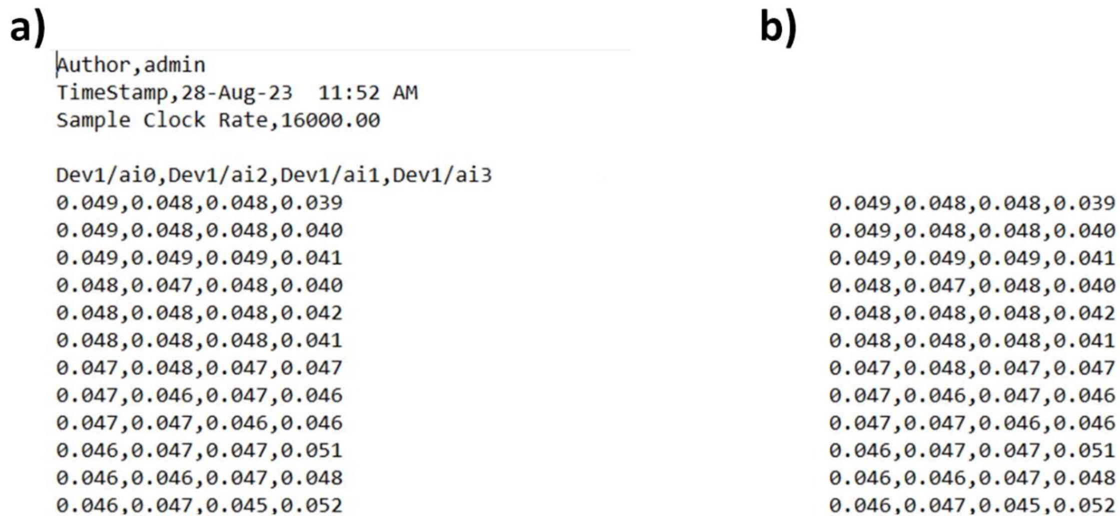

a)

```
Author,admin
TimeStamp,28-Aug-23  11:52 AM
Sample Clock Rate,16000.00

Dev1/ai0,Dev1/ai2,Dev1/ai1,Dev1/ai3
0.049,0.048,0.048,0.039
0.049,0.048,0.048,0.040
0.049,0.049,0.049,0.041
0.048,0.047,0.048,0.040
0.048,0.048,0.048,0.042
0.048,0.048,0.048,0.041
0.047,0.048,0.047,0.047
0.047,0.046,0.047,0.046
0.047,0.047,0.046,0.046
0.046,0.047,0.047,0.051
0.046,0.046,0.047,0.048
0.046,0.047,0.045,0.052
```

b)

```
0.049,0.048,0.048,0.039
0.049,0.048,0.048,0.040
0.049,0.049,0.049,0.041
0.048,0.047,0.048,0.040
0.048,0.048,0.048,0.042
0.048,0.048,0.048,0.041
0.047,0.048,0.047,0.047
0.047,0.046,0.047,0.046
0.047,0.047,0.046,0.046
0.046,0.047,0.047,0.051
0.046,0.046,0.047,0.048
0.046,0.047,0.045,0.052
```

Figure 3. Example of CSV file obtained by portable DAQ for the external construction of the topography.

The next step is to read the modified CSV file (Figure 3b) in Python to graph the frame, line, pixel, and z signals, as depicted in Figure 4.

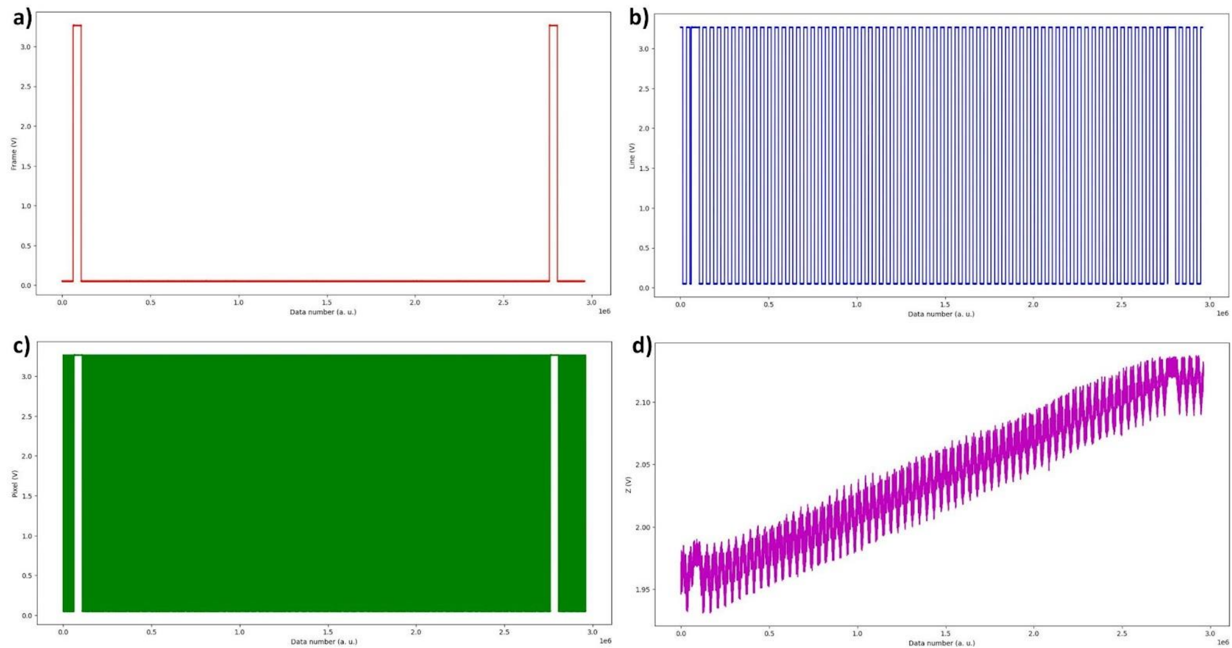

Figure 4 Topography and signals obtained on hard disc by AFM contact mode. a) Frame, b) Line, c) Pixel, and d) z.

First, the frame signal will be analyzed. The frame (Figure 4a) shows two zones where the voltage (Frame is in volts) is up to 3V. These zones are associated with the start and end of the image, as depicted in Figure 5 (red lines). To identify the exact data points where these voltages differ from zero, the concept of numerical derivative or a command that utilizes this concept in the Python code is employed.

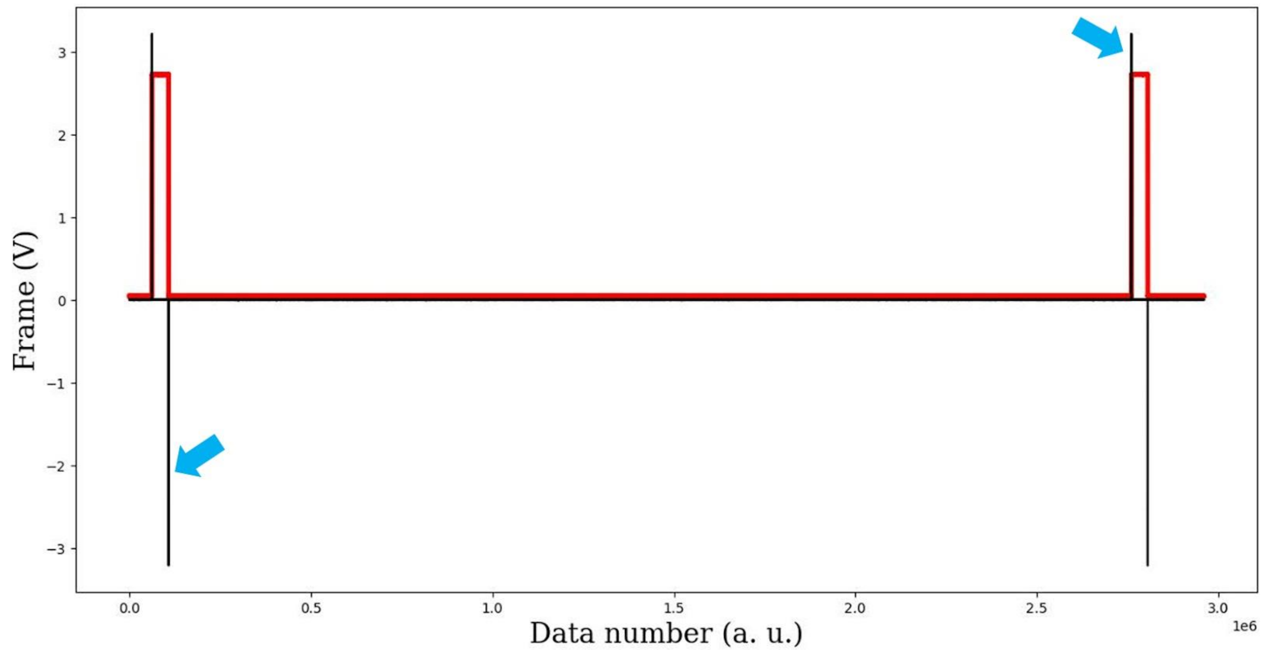

Figure 5. The frame in red and its derivative in black, the blue arrows indicate the start and end of the image.

In Figure 5, four vertical black lines indicate changes in the frame signal. The blue arrows highlight the black lines, indicating the start and end of the image. In the region delimited by the blue arrows, the line signal will be analyzed, as this zone contains all the information of our image.

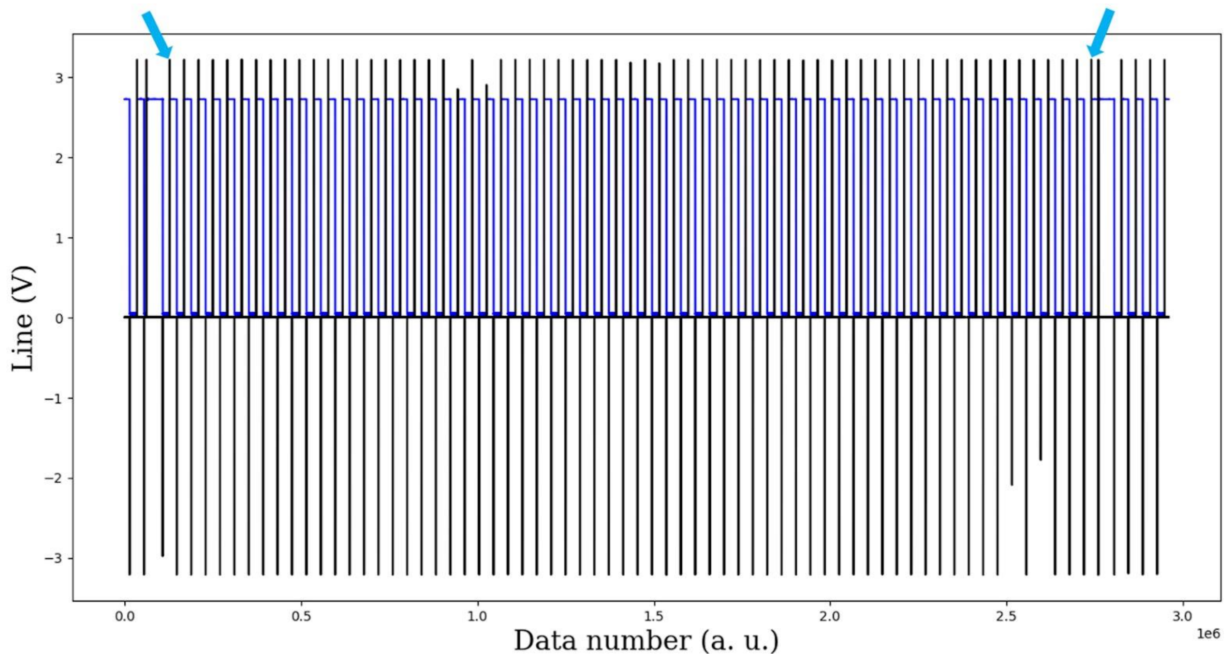

Figure 6. The line signal in blue and its derivative in black, the blue arrows indicate the start and end of the image.

Figure 6 displays the line and its derivative, with the derivative marking the start and end of the lines. Only positive derivatives will be utilized to construct the image of 64 lines, in accordance with the frame where the image is limited by the lines selected by the blue arrows.

The next step involves analyzing the pixel signal. In Figure 7, the pixel signal is depicted in green, while the derivative of the lines is represented by the black line. A line (data between two positive derivative lines) comprises the forward and backward data, and the image can be constructed by utilizing either the forward or backward data. In our case, the forward data will be utilized.

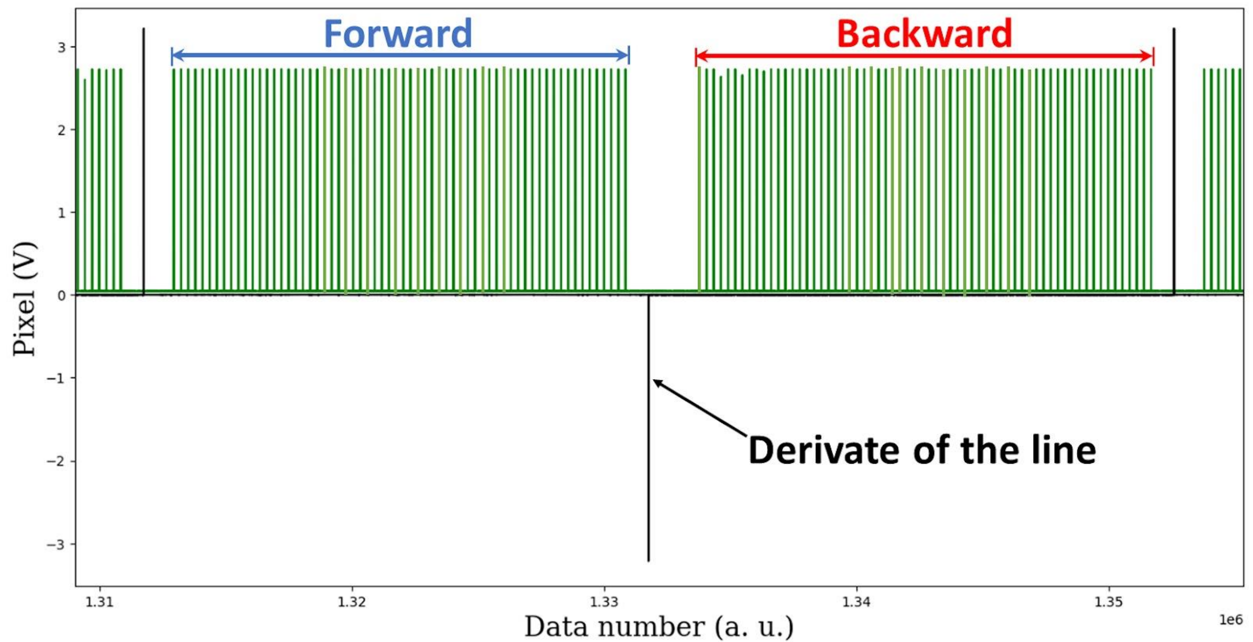

Figure 7. The forward and backward pixel signal in green and the derivative of the line in black.

There are 65 pixels per line, forming 64 spaces between them, for forward or backward data. Depending on the DAQ used and its configuration, there may be a loss of pixel data. If this occurs, an additional step is necessary to reconstruct the pixels using the positions of the pixels measured as reference.

To determine the beginning and ending positions of the pixels, it is necessary to obtain the derivative of the pixels. This allows for the creation of a graph as shown in Figure 8.

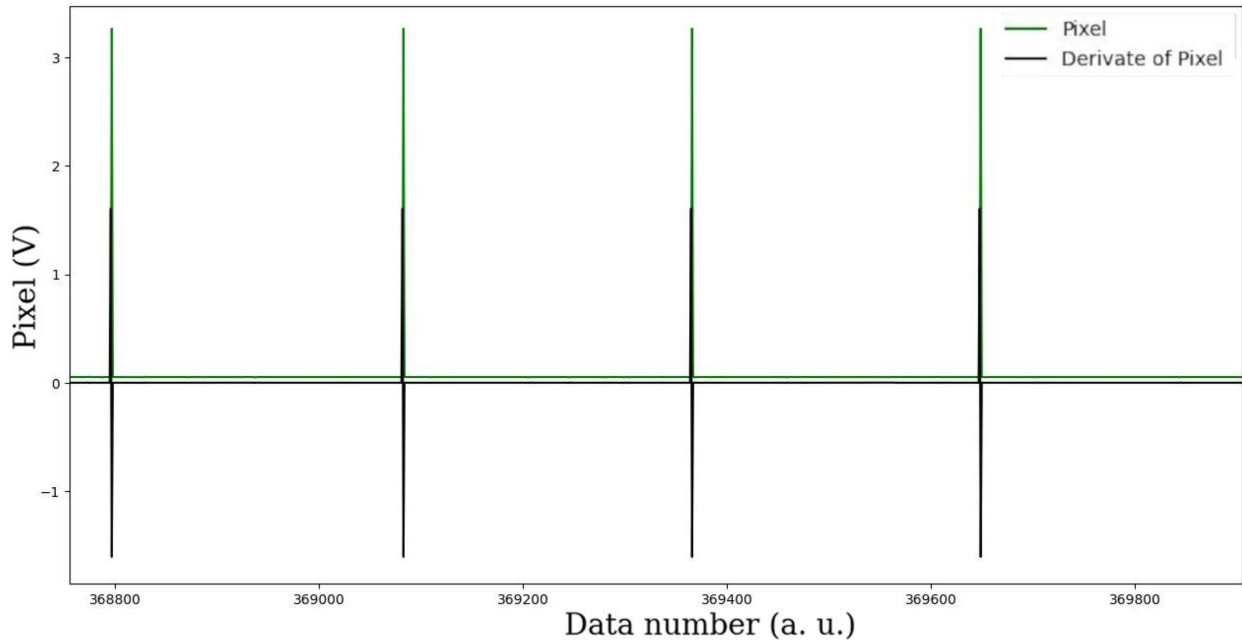

Figure 8. The pixel signal in green and its derivative in black.

The next step is to analyze the z signal, considering the position of the forward pixels. Figure 9 displays the z signal (topography in magenta) and the pixels in green. The topography exhibits variations of less than 10 mV. To construct the image of 64 pixels x 64 pixels, only one topography data point between every pixel is required. The average of the data between each pixel is useful; with this data, the 64 pixels x 64 pixels image can be constructed. It is important to note that between every pixel, there exist several topography data points. When utilizing images generated directly from AFM systems, these data points are not displayed. For certain studies, the inclusion of these data points could be crucial for thorough analysis.

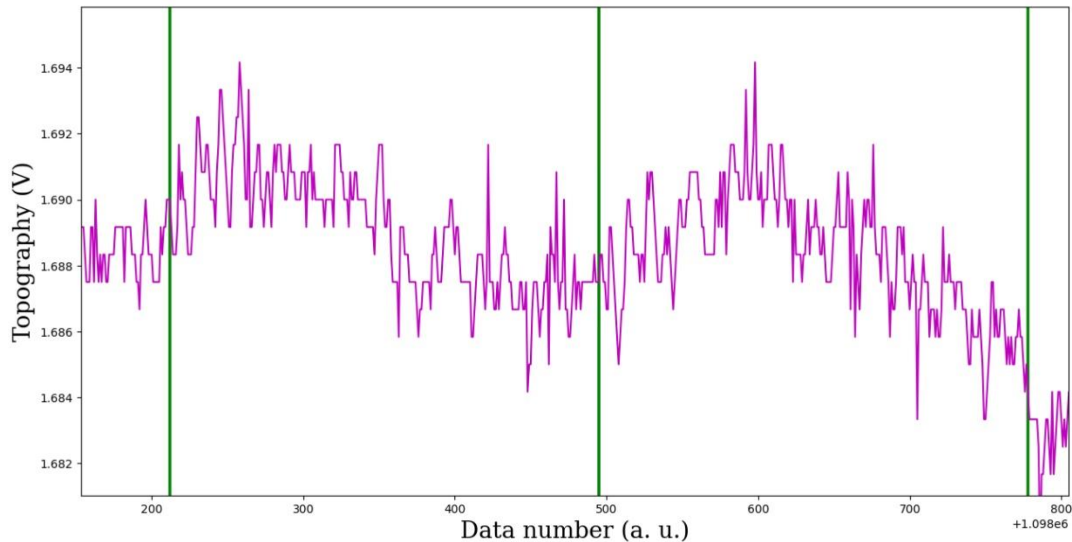

Figure 9. The forward z signal in magenta and the pixels in green.

Figure 10a displays the 3D image generated in Python by averaging the z value in every pixel. However, as observed in the image, there is a slope (also seen in Figure 4d), which is attributed to the nonlinearity of the piezoelectric components that move the AFM xy and z scanners. The "detrend" command in Python is utilized to correct this slope, which fits a polynomial to flatten the image, specifically a polynomial of degree 1, i.e., a line. Following this process, the topography image resembles Figure 10b.

Figure 10c presents the 2D topography of the hard disk, where a profile shown in Figure 10d was captured in the middle of Figure 10c in line 32.

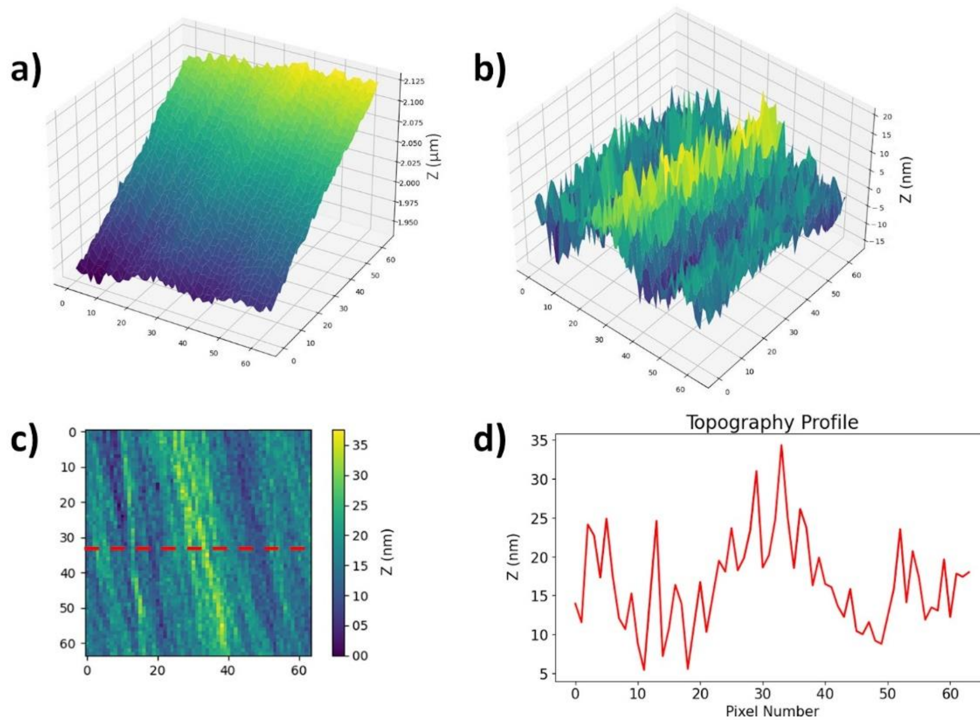

Figure 10. The forward hard disk topography obtained from the average of z in every 64 pixels x 64 pixels, a) without flatten, b) with flatten, c) 2D image of the hard disk topography and, d) topography profile.

Figure 10b is 64 pixels x 64 pixels, but a standard image in AFM is typically about 256 pixels x 256 pixels. The same procedure as above can be carried out to obtain an image of 256 pixels x 256 pixels, as shown in Figure 11. In 11a, the 3D topography of the hard disk surface is depicted, while in Figure 11b, the 3D topography obtained from the surface of the calibration grid is observed. It is more typical to display the topography images in 2D with a false color scale bar, as shown in Figures 11c and 11d; these images can be obtained in Python.

The profile of the topography in Figure 11e shows more details of the hard disk surface than the profile at 64 pixels x 64 pixels (Figure 10d). The topography profile

of the calibration grid (Figure 11f) reveals rectangles with a height of around 115 nm, which is consistent with the 111 nm of this standard grid HS-100MG.

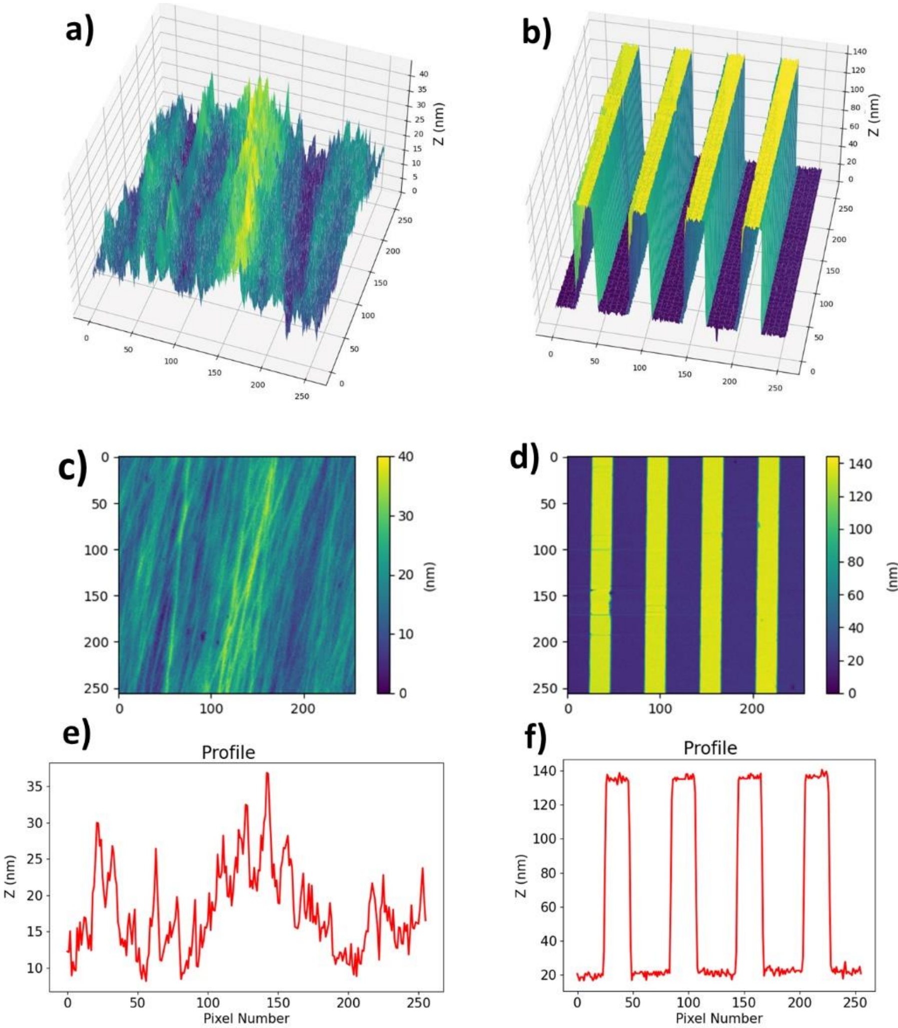

Figure 11. 3D topography of a) hard disk and b) calibration grid HS-100MG; 2D topography of c) hard disk and d) calibration grid HS-100MG; topography profile of e) hard disk and f) calibration grid HS-100MG.

The z units are in volts because the acquisition is done by the DAQ. To convert the z units to nanometers, it is necessary to obtain the inverse optical lever sensitivity

(invOLS) from the slope of a force vs. distance curve measured on an incompressible surface, such as silicon.

AFMDAQ Acquisition.

AFMDAQ Acquisition is a program developed to acquire raw data from the AFM using an NI USB-6356 DAQ. It features a graphical user interface (GUI) that facilitates establishing a connection with the DAQ and provides options to set the sampling frequency and the number of samples. The interface includes buttons for initializing and stopping sampling, as shown in Figure 12. Additionally, it prompts the user to specify the name under which the acquired data will be saved. The data is stored in a CSV file format for further processing. AFMDAQ Acquisition software enables the acquisition of six channels of data: frame, line, pixel, topography, data1, and data2. The latter two channels, data1 and data2, can be utilized for acquiring physical properties data such as friction or lateral signals (forward and backward), or piezoresponse amplitude and phase signals, as will be discussed later. To run the AFMDAQ Acquisition GUI program, the *nidaqmx* Python package is necessary.

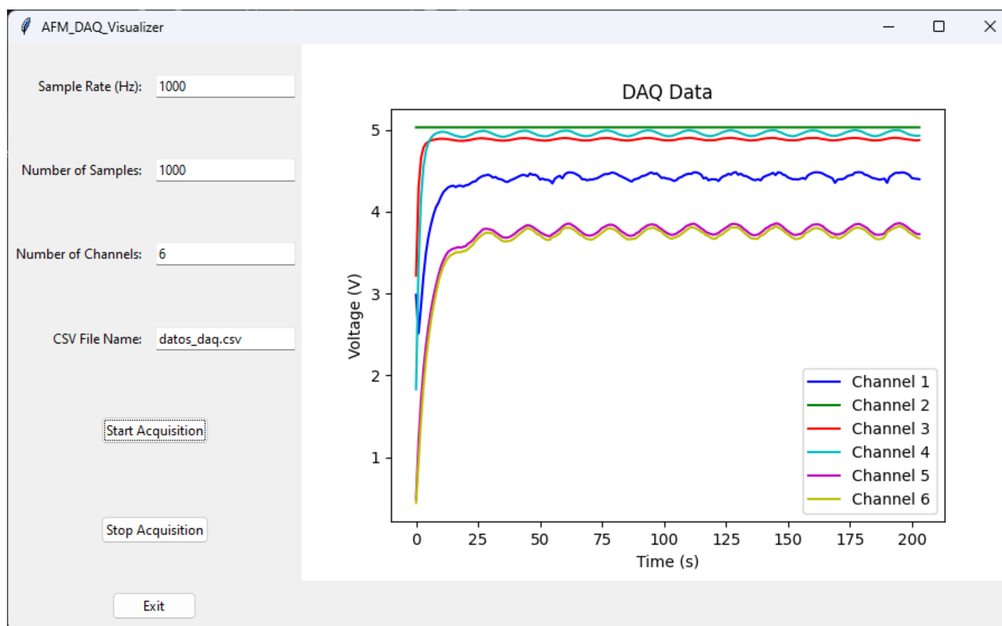

Figure 12. AFMDAQ acquisition GUI.

AFMDAQ Visualizer: Graphical user interface.

AFMDAQ Visualizer is a graphical user interface (GUI) designed to process the CSV files acquired using the AFMDAQ Acquisition program. The AFMDAQ Visualizer GUI allows the user to first select the path to the previously saved CSV file. Then, the user must choose one of the three types of microscopy that the program can currently process: Topography, PFM, and Force-Time Curves from the Force-Volume AFM Mode. Once this selection is made, the user must specify the pixel resolution of the microscopy from which the CSV data originates. This resolution is typically indicated as "n x n," for example, 64 x 64, 128 x 128, 256 x 256, and so on.

Depending on the previous configuration, a checkbox list will be displayed, showing the available options for plotting Table 1, for more details see Figure S1 supporting information:

Table 1. Options for images and graphics of the AFMDAQ Visualizer software.

Topography	Piezoresponse Force Microscopy (PFM)	Force-time curves
• 3D Topography • 2D Topography • Topography line profile	• 2D Topography • 2D Amplitude • 2D Phase • 3D Topography • 3D Amplitude • 3D Phase • Topography line profile • Amplitude line profile • Phase line profile	• Forward • Backward • Forward line profile • Backward line profile • Adhesion energy.

Both programs are available on the GitHub site https://github.com/Monopolo-Magnetico/AFM_DAQ_Visualizer. Additionally, the software was tested on the Bruker/Veeco/Digital Instruments Nanoscope IV Dimension 3100 AFM to verify that the programs function effectively on every scanning probe microscope system with access to the frame, line, pixel, and topography signals (see Figure S2 and S3 in the supporting information).

Image reconstruction of physical properties measured by atomic force microscopy by using external portable data acquisition card.

To test the AFMDAQ Acquisition and AFMDAQ Visualizer programs, piezoresponse force microscopy, force volume mapping and friction force microscopy were carried out.

- **Piezoresponse force microscopy**

Piezoresponse force microscopy (PFM) is employed to map the distribution of domains and domain walls in ferroelectric samples. To conduct PFM, a lock-in amplifier is necessary to derive the domain and domain wall information from the PFM amplitude and PFM phase. The setup for the PFM experiment is depicted in Figure 13. In PFM, a conductive cantilever is utilized because electrical fields are applied to the sample through it.

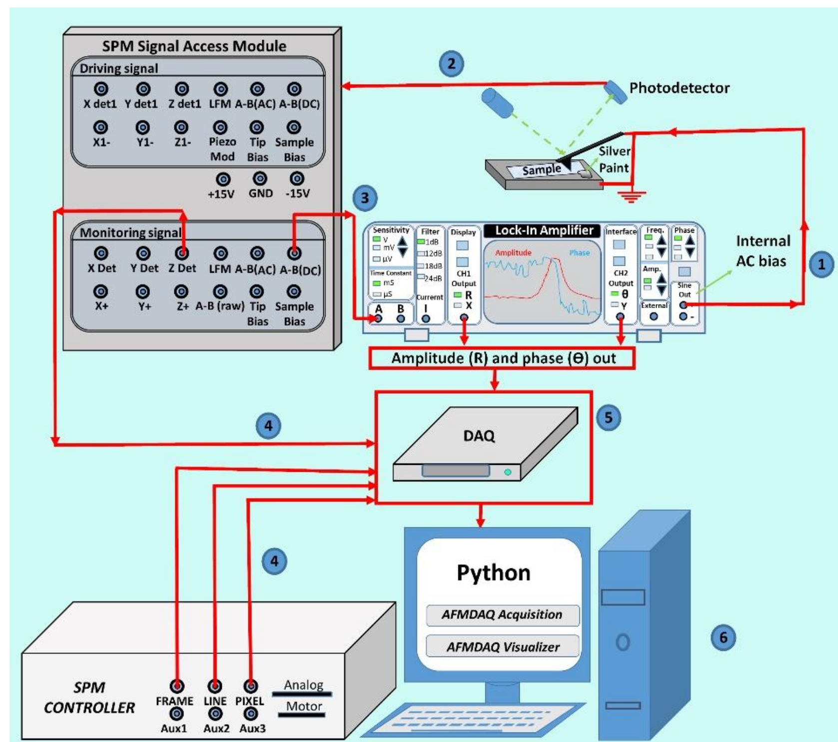

Figure 13. Piezoresponse force microscopy setup by using external data acquisition card.

The PFM experiment relies on detecting the electromechanical response of the ferroelectric sample due to the inverse piezoelectric effect, achieved by applying an

AC field to the sample through a conductive cantilever. The steps to carry out the PFM experiment are as follows: First, an AC bias from the lock-in amplifier is applied to the sample, which contains a grounded reference electrode, as shown in step 1 of Figure 13. This AC bias induces deformations in the ferroelectric material. The second step involves accessing the electromechanical behavior of the sample by monitoring the deflection signal (A-B(DC)) from the signal access module (step 2, Figure 13). The cantilever deflection (A-B(DC)) signal provides information on the small deformations of the sample, which is then sent to the lock-in amplifier for comparison with the applied AC bias (step 3, Figure 13). The lock-in amplifier cleans and amplifies the electromechanical behavior of the ferroelectric sample. From the lock-in amplifier, signals of amplitude and phase are obtained, which are recorded by the DAQ (step 4, Figure 13). Simultaneously, the z, pixel, line, and frame are acquired by the DAQ, and the data are saved in the computer by using the AFMDAQ Acquisition GUI program (steps 4 and 5, Figure 13). By following the procedure described above, the topography, amplitude PFM, and phase PFM images can be reconstructed using the AFMDAQ Visualizer software (step 6, Figure 13). The phase and amplitude PFM signals are shown in Figure 14 a and b.

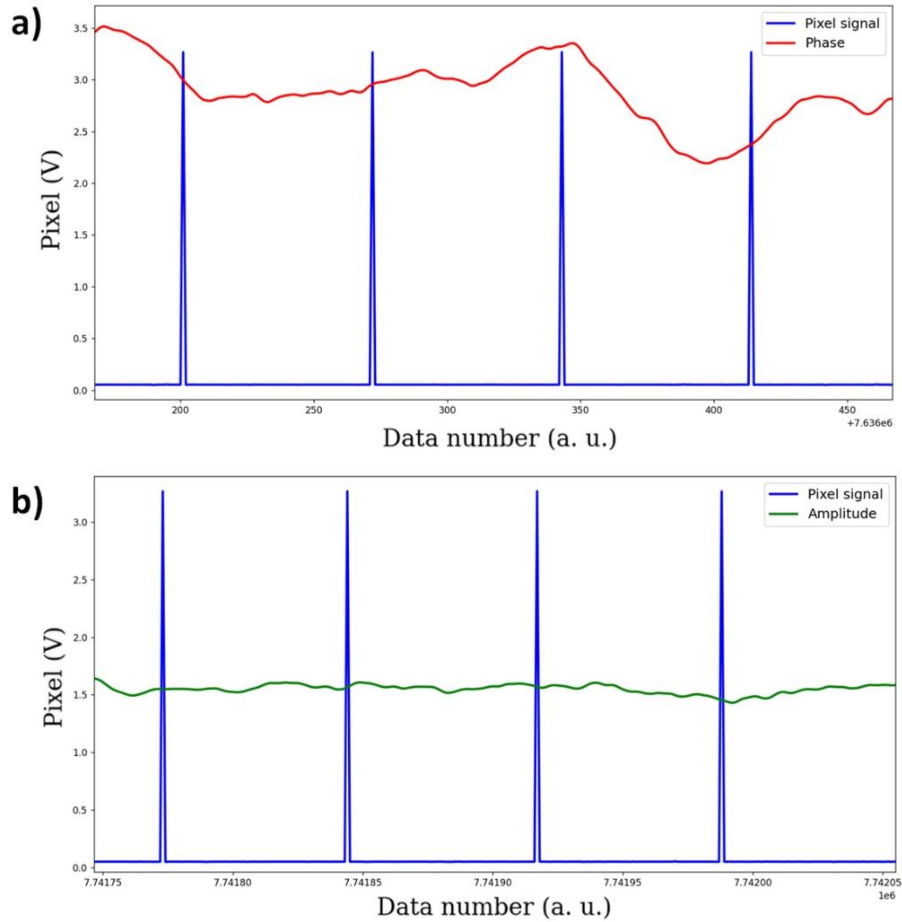

Figure 14. The pixel signal in blue and a) phase in red and b) amplitude in green.

The topography and PFM images obtained and reconstructed by using the AFMDAQ Visualizer software are shown in Figures 15a, 15b, and 15c. The figure 15a reveals the low roughness of the surface on the $LiNbO_3$ sample. The amplitude and its profile display the domain walls in figure 15b, while the phase illustrates two different regions with opposite polarization, as seen in figure 15c.

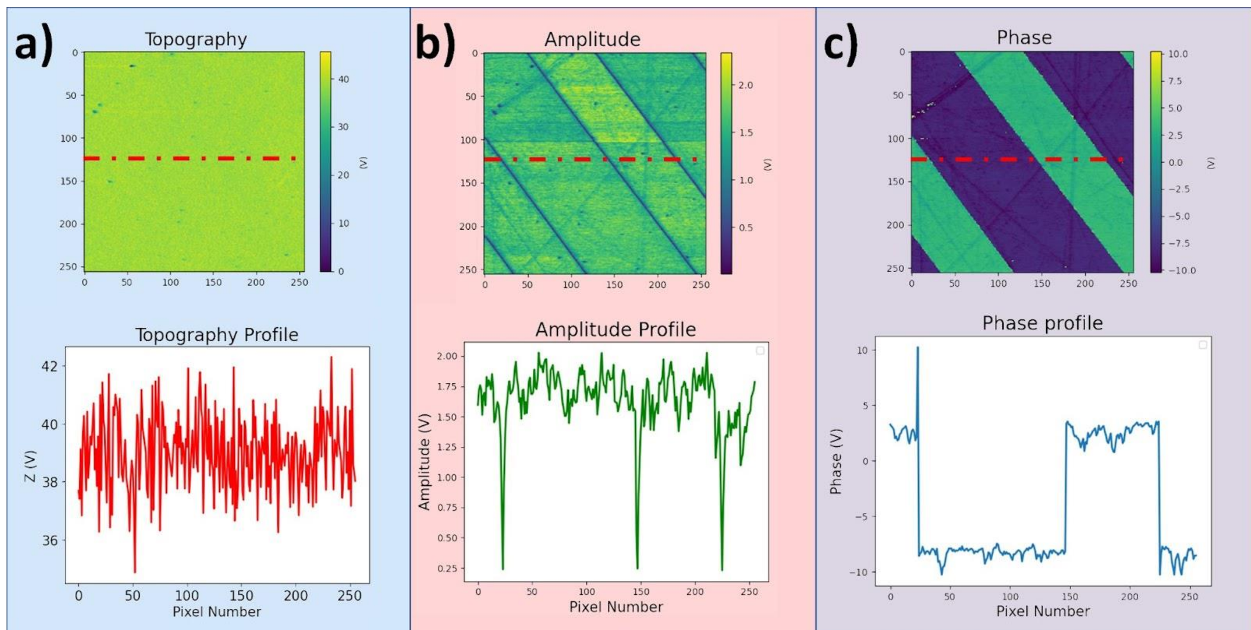

Figure 15. Reconstructed 2D images of a) Topography b) Amplitude PFM and, c) Phase PFM and down its respective profile taken from the red dotted line. Data obtained by using the PFM setup and the procedure described above on a $LiNbO_3$ periodically-poled reference ferroelectric sample.

- **Force Volume Mapping.**

In force volume mode (FVM), a force-distance curve is obtained pixel by pixel along the surface scanning, as illustrated in Figure 16. In this mode, lateral or frictional forces are avoided, allowing FVM to measure the surface of soft samples and obtain their mechanical properties. To prepare the sample, fresh blood drops were placed onto a glass slide and spread evenly using another glass slide, immediately the sample can be measured.

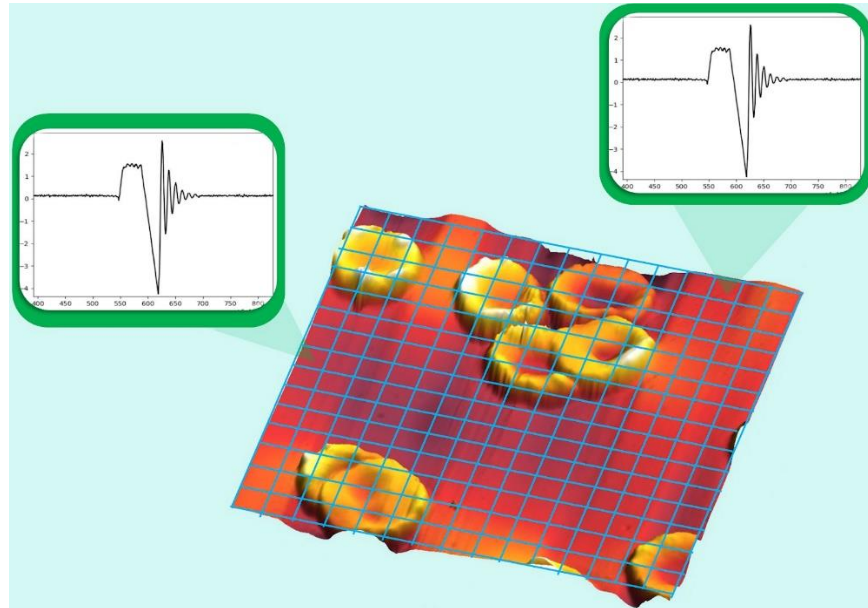

Figure 16. The force volume AFM mode, the force vs time is obtained pixel by pixel on red bood cells (the red blood cells used in the FVM experiment were donated by Jose Juan Gervacio Arciniega).

For external measurements of FVM, it is necessary to connect the channels of z (topography), the A-B (cantilever deflection), the frame, line, and pixel to the DAQ, as shown in Figure 17, and by using the AFMDAQ acquisition software.

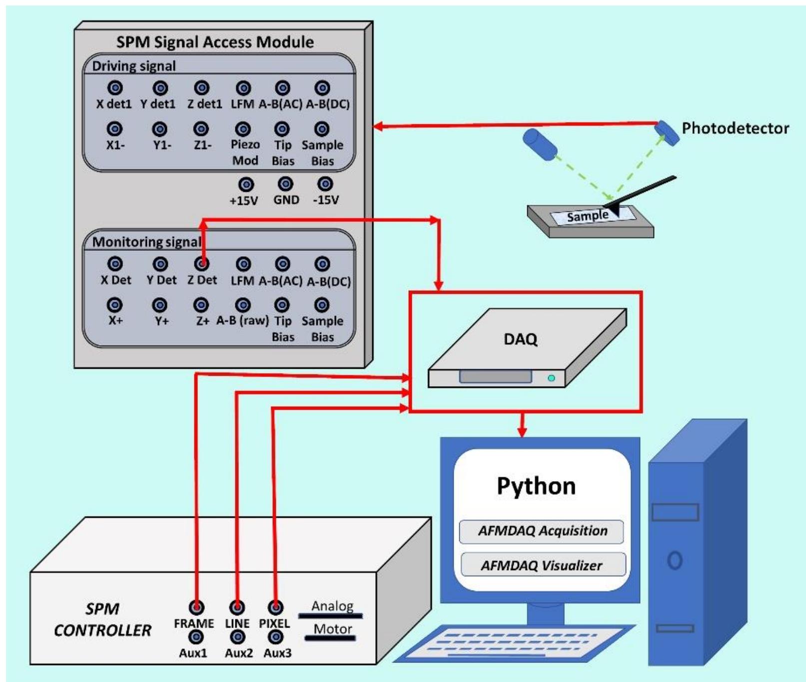

Figure 17. Force volume mapping setup by using external data acquisition card.

By following the procedure described above, the topography and adhesion force images of red blood cells can be reconstructed using the AFMDAQ Visualizer software. For the adhesion force curve, the minimum value has been calculated in every pixel as is shown in Figure 18a. More details of the sample can be observed in the adhesion force image (Figure 18c) by comparing it with the topography (Figure 18b). Through a deep analysis of the data, it is possible to extract more information from these force curves, as demonstrated in the ringing AFM mode [2].

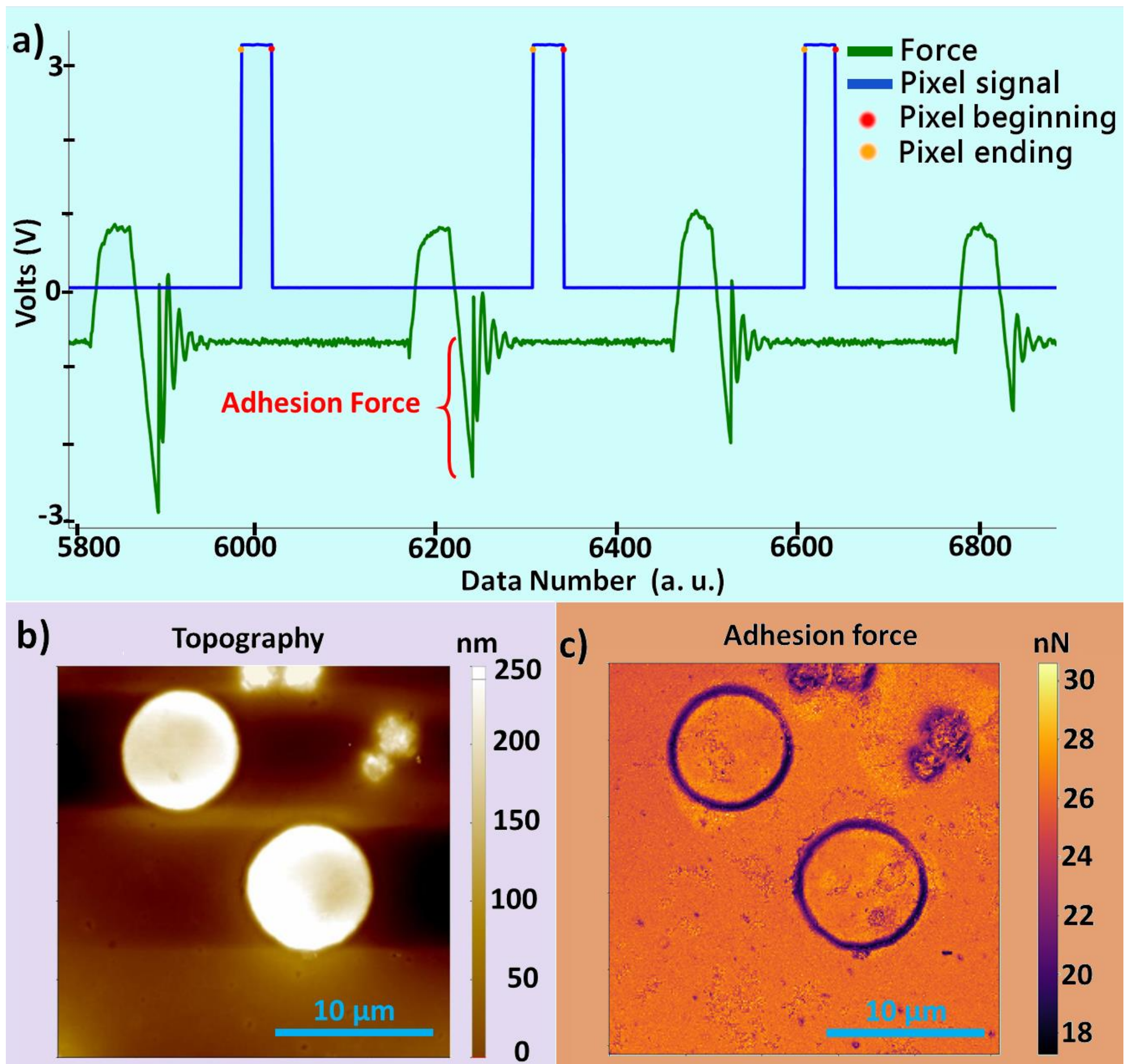

Figure 18. Force volume mapping on red blood cells sample. a) pixel and force raw data, b) topography on an area of 25 µm X 25 µm, and c) adhesion force obtained from the force-time curves.

- **Friction Force Microscopy**

Friction measurement using AFM is a technique employed to analyze the friction between the tip and the sample surface at the nanoscale. This method involves scanning a surface in contact mode and monitoring the forces experienced by the tip as it encounters different regions. By quantifying the lateral or vertical forces, it is possible to obtain valuable insights into material properties, surface topography, and the frictional behavior of nanomaterials. AFM-based friction measurements have widespread applications in fields such as materials science, tribology, and nanotechnology, providing a detailed understanding of surface characteristics and facilitating the design of materials with tailored frictional properties. Ruan and Bhushan [23] developed a method to obtain the dynamic coefficient of friction using the height mode when the scanning direction of the surface is parallel to the longitudinal axis of the cantilever, as shown in Figure 19.

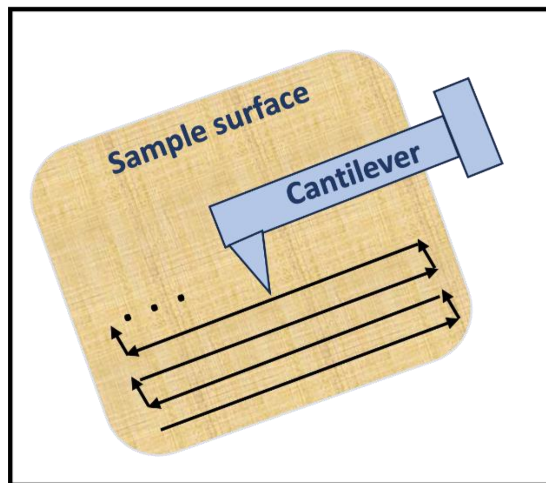

Figure 19. Parallel scanning direction while vertical information of photodetector is acquired.

During the scanning process, the Frame, Line, Pixel, and A-B (deflection signal) signals are acquired using the DAQ, see Figure 20. While scanning the surface of the sample, the set-point is incrementally raised at equal intervals along each line. The image resolution was set at 256 x 256 pixels, such that every 25 lines, the set-point was increased, resulting in a total of 10 different variations. For this analysis, the set-point was varied from 5nN to 50 nN in increments of 5nN. The ElectriCont-G cantilever from Budget Sensors and a single side polished <100> N-type Silicon sample were utilized for this experiment.

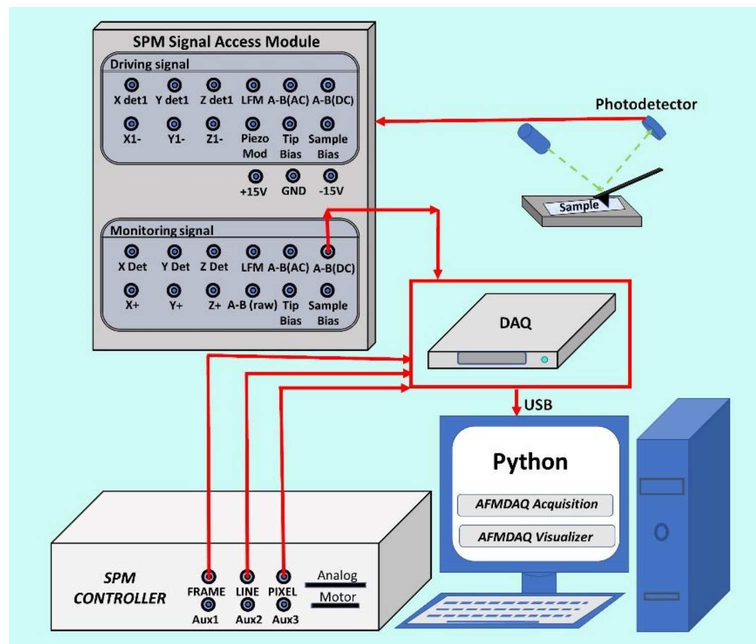

Figure 20. Setup to acquire friction signal using external data acquisition card.

Once the set-point was varied at fixed intervals during image acquisition, the obtained voltage values were then plotted, as shown in Figure 21. The set-point intervals can be distinguished in the resulting image.

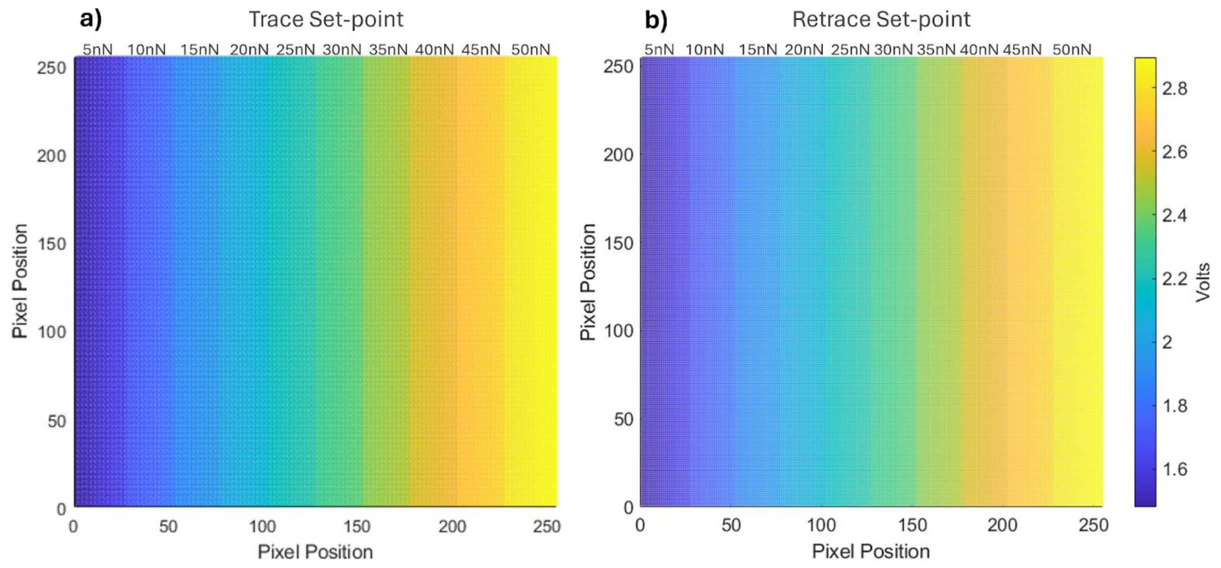

Figure 21. Trace and Retrace data signals after varying the set-point 5nN every 25 lines.

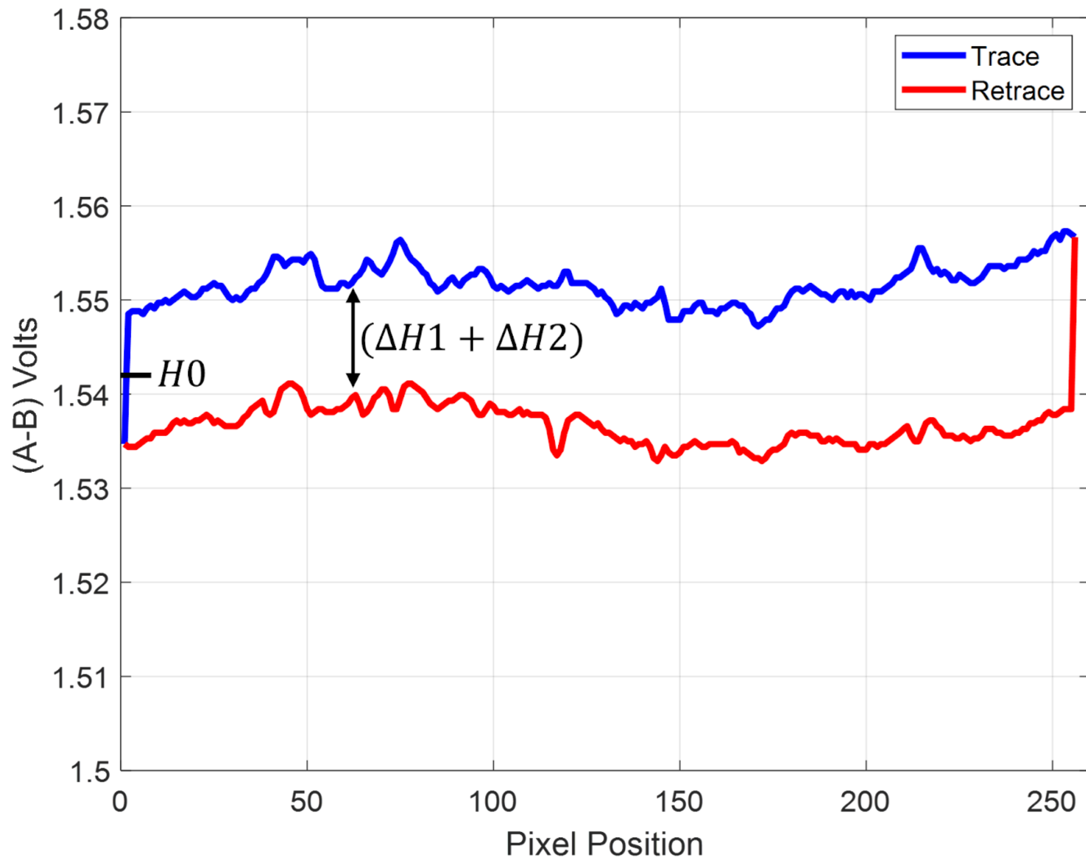

Figure 22. Trace and retrace profiles of vertical deflection of the cantilever as the sample is scanned back and forth with 5nN of set-point.

For each set-point interval, the values of H_1 and H_2 were extracted from the trace and retrace signals, respectively, along with the value of H_0, as depicted in Figure 22. With these values, the graph in Figure 23 was constructed.

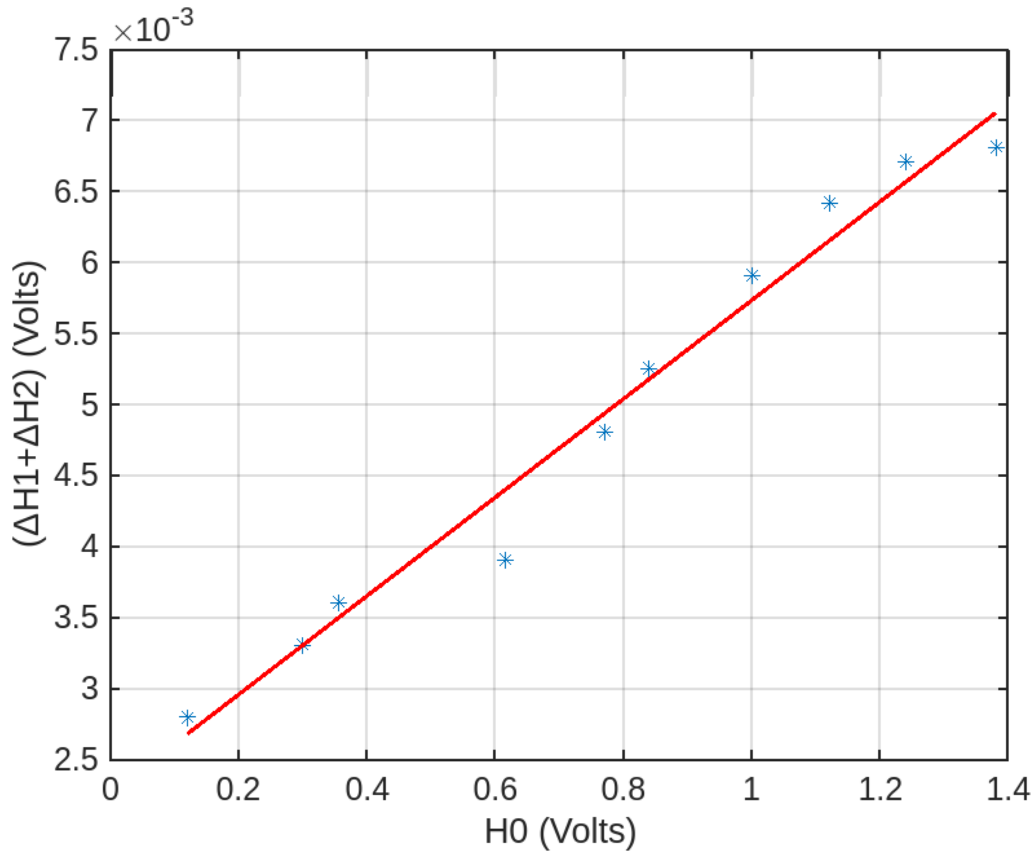

Figure 23. Vertical height difference as a function of the center position between the two traveling directions.

A linear fit was performed, resulting in a slope of 0.0035. The dimensions of the cantilever used are L = 450 μm and l = 17 μm. The following equation was used to calculate the coefficient of friction.

$$\mu = \frac{(\Delta H_1 + \Delta H_2)}{\Delta H_0} * \frac{L}{2l} = (0.0035) * \frac{450\ \mu m}{2(17\mu m)} = 0.046$$

The resulting value of the kinetic friction coefficient was 0.046, which is consistent with the value reported by Ruan, J.A &, Bhushan [23].

Conclusions

In this study, we have outlined a detailed procedure for acquiring and processing data required to construct topography images using AFM. This process involves utilizing an external acquisition card to gather the necessary data. Furthermore, we have demonstrated the versatility of this procedure in constructing images depicting physical properties such as ferroelectric domains and domain walls using PFM, adhesion force images derived from force-distance curves analysis, and the determination of the kinetic friction coefficient through FFM. The AFMDAQ acquisition and the AFMDAQ Visualizer analysis programs developed in python were showed. Importantly, our procedure and software are adaptable for the development and implementation of new external microscopies across various AFM systems. The CSV raw data files obtained through the external acquisition card adhere to a standard format, facilitating result comparison between different AFM systems. Moreover, the methodology developed herein serves as an educational tool, offering new users insights into the intricate workings of AFM. This work contributes to the broader understanding and application of AFM in diverse scientific and engineering contexts by providing a comprehensive framework for data acquisition and analysis.

Materials and Methods

The materials used in this manuscript are primarily the AFM tips and the samples, which will be described shortly:

The cantilever used for the topography of the standard calibration grid, piezoresponse force microscopy, force volume mapping, and friction force microscopy measurements is the ElectricCont-G cantilever from Budget Sensors (https://www.budgetsensors.com/contact-mode-afm-probe-platinum-electricont).

The calibration grid HS-100MG sample is a height calibration standard with a 100nm step height. It was purchased from Budget Sensors at https://www.budgetsensors.com/height-calibration-standard-hs-100mg.

The piezoresponse force microscopy (PFM) measurements were carried out using a $LiNbO_3$ sample obtained from Oxford Instruments, AR-PPLN test sample ID 900.241 (https://estore.oxinst.com/uk/products/microscopy-supplies/atomic-force-microscopy/zid900.241). This sample is a periodically polarized ferroelectric sample with opposite out-of-plane polarized domains. The PFM measurement was carried out in resonant mode by applying an AC voltage of 1Vpp at 208 kHz, near the second resonant frequency.

For the force volume mapping, blood cells donated by Jose Juan Gervacio were used. A drop of blood was extracted from Jose Juan Gervacio's index finger by pricking it with a clean needle. The fresh blood drop was placed onto a glass slide and spread evenly using another glass slide. The sample was measured immediately. The force mapping was carried out by applying a maximum force of 70nN in a scan of 256 pixels x 256 pixels over an area of 25 x 25 μm^2.

For the friction force microscopy, a single-side polished <100> N-type Silicon sample (purchased from Sigma Aldrich, https://www.sigmaaldrich.com/MX/es/product/aldrich/646687) was utilized. The sample was cleaned using an acetone and alcohol ultrasonic bath.

All the AFM experiments were carried out using the XE-7 atomic force microscope from Park Systems. An additional topography measurement was obtained using a Bruker/Veeco/Digital Instruments Nanoscope IV Dimension 3100 AFM to test the AFMDAQ Visualizer software.

Additionally, the atomic force microscope and the data acquisition systems are two important instruments essential for this work. Details of these instruments are described below.

Atomic Force Microscope

The atomic force microscope (AFM) is a pivotal tool utilized for characterizing the morphology and physical properties of materials at the micro and nanoscale. The AFM employs a sharp tip positioned at one end of a microbeam called a cantilever. The atoms at the tip's edge interact with the surface atoms of the sample, causing deflections in the cantilever. These deflections are detected by a photodetector array through a laser beam that reflects off one side of the cantilever, a system known as optical beam deflection (OBD). The signals captured by the photodetector serve two main purposes: 1) reconstructing the topography or certain physical properties of the

sample, and 2) aiding the feedback system to maintain scanning conditions dependent on the operational mode of the AFM.

For morphology measurements with AFM, only a Si or NiSi cantilever is necessary. However, when measuring physical properties, cantilevers with specialized coatings become essential. For instance, to measure magnetic properties, a cantilever with a Cr/Pt coating may be used. For electric and piezoelectric properties, a cantilever with a conductive coating is employed. To measure mechanical properties, a cantilever with a hard coating such as diamond-like carbon is necessary. For measuring biological samples, cantilevers coated with inert materials such as gold are used to avoid reactions and changes with the live samples.

The AFM photodetector typically comprises four areas, as depicted in Figure 24. The vertical signals or vertical bending of the cantilever can be detected by the signal (A+B)-(C+D)/(A+B+C+D) see Figure 24a. While the lateral signals or torsion of the cantilever are obtained from: (A+C)-(B+D)/(A+B+C+D) see Figure 24b.

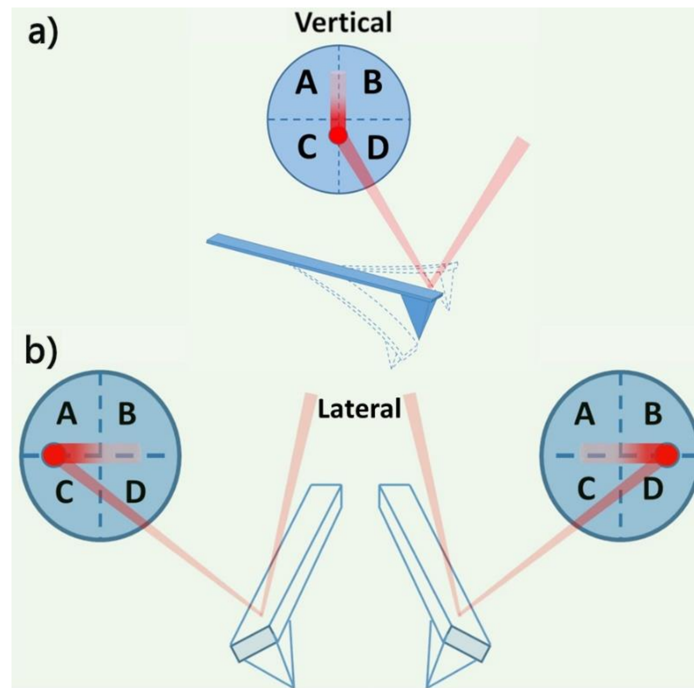

Figure 24. a) Vertical and b) Lateral cantilever AFM movement detection by the photodetector.

The access to the photodetector signals allows for tracking the various interaction forces between the AFM tip and different samples. The photodetector's vertical and lateral signals can be obtained through the signal access module (SAM), or in some cases, these signals may be accessible through the scanning probe microscope (SPM) controller (this depends on the SPM company). When developing new AFM microscopies, it is crucial to determine the accessibility of the photodetector's vertical and lateral signals in each specific case.

For the XE-7 Park System SPM, the SAM is illustrated in Figure 25a. The SAM comprises two signals: the driving signal and the monitoring signal. For the purposes

of this study, the monitoring signals will be utilized, particularly the photodetector's vertical signal (AFM deflection) labeled as A-B(AC) in Figure 25a.

On the other hand, from the SPM controller, the signals for frame, line, and pixel will be obtained for the construction of topographic images (refer to Figure 25b). The frame signal denotes the beginning and end of an image, the line indicates the beginning and end of a line, and the pixel signifies the beginning and end of one pixel. These signals are depicted in Figure 25b. Further ahead, the utilization of frame, line, and pixel signals for externally constructing topography will be elucidated.

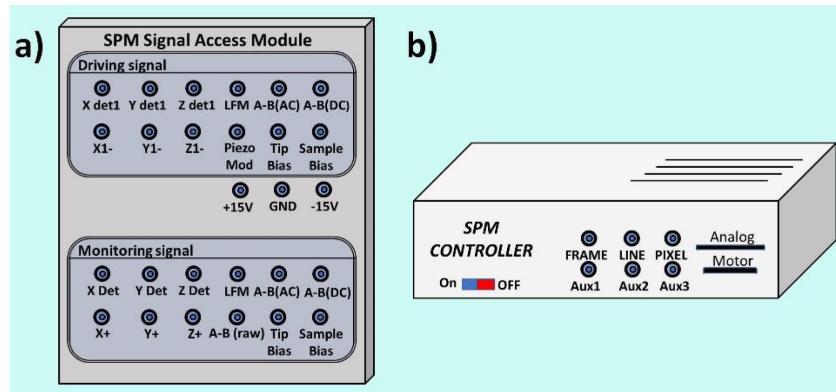

Figure 25. a) Signal access module (SAM), b) Rear side of the controller XE-7 SPM from Park Systems.

Data Acquisition System selection

A data acquisition system (DAQ) is a combination of hardware and software designed to sample a physical parameter, such as voltage or current, and convert it into a digital signal that can be stored in a computer for analysis.

It is crucial to choose a DAQ properly according to the requirements of the measurement system to be implemented. The specific parameters required of a DAQ depend entirely on the number of analog input channels, resolution, and sampling rate. The most important characteristics to consider in a DAQ include resolution, accuracy, sampling frequency, number of channels to be monitored, analog or digital channels, and the number of analog-to-digital converters [24].

DAQs can be classified based on their sampling rate and portability. The most portable are those that utilize the USB protocol to transmit data to a computer, followed by cards that connect to a desktop computer's bus, and finally, those with their own internal computer, rendering them stand-alone systems, such as PXI (PCI Express Extension) systems see Figure 26.

Portable DAQs are cost-effective, easy to configure, and utilize the USB protocol for data communication with a computer. Moreover, certain versions of this type of DAQ utilize the same voltage as the USB interface to power their internal circuitry, eliminating the need for an external power supply. These data acquisition boards are equipped with analog inputs and outputs, digital inputs and outputs, and timers. However, the primary drawback of these cards is their lack of high precision. Additionally, their sampling rate is constrained by the speed of the USB protocol, and they are not engineered to function in industrial environments.

Desktop DAQs can be installed in a PCI (Peripheral Component Interconnect) or PCIe (PCI Express) bus of a desktop computer. They offer the advantage of

leveraging the bus speed, while maintaining signal integrity through shared grounding with the computer chassis.

For high performance, PXI (PCI Express Extension) Systems are recommended due to their high measurement throughput and proven ability to reduce test time and overall costs. The combination of high performance, modularity, and software connectivity makes them ideal for test applications requiring high accuracy, extensive channel counts, and mixed measurements.

The selection of a data acquisition card is a crucial decision in measurement and control systems, directly impacting data fidelity and system efficacy. To make an informed choice, multiple pivotal factors must be considered, harmonized with the specific requirements of the application. These factors include sampling rate, resolution, quantity of analog and digital channels, and the necessity of either a differential or ground-referenced signal.

The sampling rate emerges as a foundational parameter, dictating the pace at which the data acquisition card can acquire data. It should be deliberated in accordance with the signal's frequency under investigation. In scenarios with high-frequency signals, such as communication applications, a sufficiently elevated sampling rate is imperative to prevent the inadvertent omission of crucial information. Conversely, when assessing low-frequency signals, opting for a card with a lower sampling rate is judicious to optimize computational resources and reduce overall costs [25].

Resolution holds paramount significance as an indispensable facet when scrutinizing data acquisition cards. Within this context, resolution pertains to the card's capacity to convert analog signals into discrete digital values. Elevated resolution endows the system with an enhanced capability to discern minute differentiations in signal values, particularly crucial in applications where precision is paramount [26]. Nonetheless, judicious balancing is requisite, as escalated resolution often demands augmented hardware resources and commensurately heightened power consumption, necessitating a nuanced equilibrium aligned with the application's requisites [27].

The quantity of analog and digital channels on a data acquisition card constitutes another element demanding fastidious contemplation. Determining an appropriate channel count is contingent upon the application's demands; applications replete with a profusion of sensors or signals necessitate the procurement of a data acquisition card offering a sufficiently extensive complement of channels. Furthermore, it is incumbent upon the investigator to gauge the necessity for analog, digital, or a judicious amalgamation of both channel types, as certain applications mandate the synchronous conversion of both analog and digital signals [28].

Moreover, the choice between differential and ground-referenced signal acquisition poses an important quandary, contingent upon signal quality and the extent of electromagnetic interference within the environment. Differential signals confer greater immunity to interference, quantifying voltage differentials between two points and thereby mitigating common-mode disturbances [29]. In settings replete with

electrical noise or where signal integrity is paramount, the selection of a card accommodating differential signals is a sagacious course of action. Conversely, in cases characterized by robust signal strength and minimal susceptibility to interference, data acquisition cards incorporating ground-referenced signals may constitute a more economically prudent alternative.

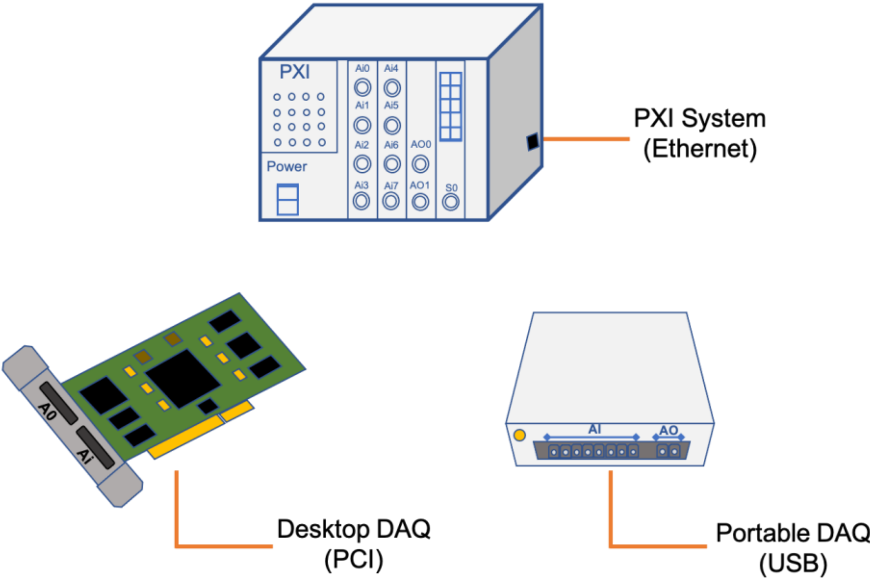

Figure 26. Different types of DAQ systems and their communication protocols.

Description of the developed software.

AFMDAQ Acquisition

The software AFMDAQ acquisition was developed in python [30] to control the DAQ and save the data in a CSV file. The parameters that can be modified are the sample rate in Hz, number of samples, number of channels from 1 to 6, the name of the csv

file, additionally has a button for start and end the data acquisition. The AFMDAQ Acquisition software display in a real time a graphic with the information channels.

AFMDAQ Visualizer

The AFMDAQ Visualizer is a tool developed in Python for easy processing of the data obtained by a DAQ and the AFMDAQ Acquisition software. The AFMDAQ Visualizer contains options for processing topography, piezoresponse force microscopy, and force-time curves. For topography, the user can choose the image size by specifying the number of pixels. Options for 2D and 3D graphics are available, and the profile along the required line can be obtained. For piezoresponse force microscopy, the pixel resolution, 2D and 3D topography, amplitude, and phase can be selected, and the profiles of these signals can be graphed. For the force-time curves, the topography and the adhesion force 2D images can be obtained for the forward and backward scans. The AFMDAQ Acquisition and AFMDAQ Visualizer can be downloaded from this link (https://na01.safelinks.protection.outlook.com/?url=https%3A%2F%2Fgithub.com%2FMonopolo-Magnetico%2FAFM_DAQ_Visualizer&data=05%7C02%7C%7C6b3795829c194467462308dc799510fc%7C84df9e7fe9f640afb435aaaaaaaaaaaa%7C1%7C0%7C638518928388466960%7CUnknown%7CTWFpbGZsb3d8eyJWIjoiMC4wLjAwMDAiLCJQIjoiV2luMzIiLCJBTiI6Ik1haWwiLCJXVCI6Mn0%3D%7C0%7C%7C%7C&sdata=NyK3WNYQymS1JdlZJz0RAwPuFyXMszhuXOsCdO09jQ4%3D&reserved=0). These software tools will be upgraded to expand the options and analysis capacity.

Acknowledgments

J. J. G. acknowledges the financial support provided by CONACYT, Mexico (Grant No. PCC-320548). Thanks to Dr. J. J. Gervacio Arciniega to donate the red blood sample for FVM experiments. Thanks are also extended to Dr. Bryan Wagner for his valuable comments, which helped enhance this manuscript.

Data availability

Examples of AFM data obtained via DAQ are available upon request.

References

1 Binnig, G., Quate, C.F., Gerber, Ch.: ‘Atomic Force Microscope’ *Phys Rev Lett*, 1986, **56**, (9), pp. 930–933.

2 Dokukin, M.E., Sokolov, I.: ‘Nanoscale compositional mapping of cells, tissues, and polymers with ringing mode of atomic force microscopy’ *Sci Rep*, 2017, **7**, (1).

3 Zeng, Q., Sim, C., Yong, A.M., *et al.*: ‘Emerging multi-frequency surface strain force microscopy’ *J Appl Phys*, 2023, **133**, (4).

4 Murillo-Bracamontes, E.A., Gervacio-Arciniega, J.J., Cruz-Valeriano, E., *et al.*: ‘Contact resonance frequencies and their harmonics in scanning probe microscopy’ *IET Science, Measurement and Technology*, 2021, **15**, (5), pp. 419–426.

5 Alikin, D., Safina, V., Abramov, A., *et al.*: ‘Defining ferroelectric characteristics with reversible piezoresponse: PUND switching spectroscopy PFM characterization’ *Nanotechnology*, 2024, **35**, (17).

6 Ramer, G., Aksyuk, V.A., Centrone, A.: 'Quantitative Chemical Analysis at the Nanoscale Using the Photothermal Induced Resonance Technique' *Anal Chem*, 2017, **89**, (24), pp. 13524–13531.

7 Piergies, N., Mathurin, J., Dazzi, A., *et al.*: 'IR nanospectroscopy to decipher drug/metal nanoparticle interactions: Towards a better understanding of the spectral signal enhancement and its distribution' *Appl Surf Sci*, 2023, **609**.

8 Li, Y., Zhang, C., Tian, Z., Cai, X., Guan, B.: 'Identification and quantification of nanoplastics (20–1000 nm) in a drinking water treatment plant using AFM-IR and Pyr-GC/MS' *J Hazard Mater*, 2024, **463**.

9 Chen, Q.N., Ma, F., Xie, S., Liu, Y., Proksch, R., Li, J.: 'High sensitivity piezomagnetic force microscopy for quantitative probing of magnetic materials at the nanoscale' *Nanoscale*, 2013, **5**, (13), pp. 5747–5751.

10 Rabe, U., Amelio, S., Kester, E., Scherer, V., Hirsekorn, S., Arnold, W.: 'Quantitative determination of contact stiffness using atomic force acoustic microscopy' *Ultrasonics*, 2000, **38**, (1–8), pp. 430–437.

11 Enriquez-Flores, C.I., Gervacio-Arciniega, J.J., Cruz-Valeriano, E., De Urquijo-Ventura, P., Gutierrez-Salazar, B.J., Espinoza-Beltran, F.J.: 'Fast frequency sweeping in resonance-tracking SPM for high-resolution AFAM and PFM imaging' *Nanotechnology*, 2012, **23**, (49).

12 Varesi, J., Majumdar, A.: 'Scanning Joule expansion microscopy at nanometer scales' *Appl Phys Lett*, 1998, **72**, (1), pp. 37–39.

13 Müller, P., Abuhattum, S., Möllmert, S., Ulbricht, E., Taubenberger, A. V., Guck, J.: ‘Nanite: Using machine learning to assess the quality of atomic force microscopy-enabled nano-indentation data’ *BMC Bioinformatics*, 2019, **20**, (1).

14 López-Alonso, J., Eroles, M., Janel, S., *et al.*: ‘PyFMLab: Open-source software for atomic force microscopy microrheology data analysis’ *Open Research Europe*, 2023, **3**, p. 187.

15 Hermanowicz, P., Sarna, M., Burda, K., Gabryś, H.: ‘AtomicJ: An open source software for analysis of force curves’ *Review of Scientific Instruments*, 2014, **85**, (6).

16 Beton, J.G., Moorehead, R., Helfmann, L., *et al.*: ‘TopoStats – A program for automated tracing of biomolecules from AFM images’ *Methods*, 2021, **193**, pp. 68–79.

17 Oxvig, C.S., Pedersen, P.S., Arildsen, T., Østergaard, J., Larsen, T.: ‘Magni: A Python Package for Compressive Sampling and Reconstruction of Atomic Force Microscopy Images’ *J Open Res Softw*, 2014, **2**.

18 Han, G., Lv, L., Yang, G., Niu, Y.: ‘Super-resolution AFM imaging based on compressive sensing’ *Appl Surf Sci*, 2020, **508**.

19 Amyot, R., Marchesi, A., Franz, C.M., Casuso, I., Flechsig, H.: ‘Simulation atomic force microscopy for atomic reconstruction of biomolecular structures from resolution-limited experimental images’ *PLoS Comput Biol*, 2022, **18**, (3).

20 Fantner, G.E., Hegarty, P., Kindt, J.H., Schitter, G., Cidade, G.A.G., Hansma, P.K.: ‘Data acquisition system for high speed atomic force microscopy’ *Review of Scientific Instruments*, 2005, **76**, (2).

21 Nečas, D., Klapetek, P.: ‘Gwyddion: an open-source software for SPM data analysis’ *Open Physics*, 2012, **10**, (1), pp. 181–188.

22 Horcas, I., Fernández, R., Gómez-Rodríguez, J.M., Colchero, J., Gómez-Herrero, J., Baro, A.M.: 'WSXM: A software for scanning probe microscopy and a tool for nanotechnology' *Review of Scientific Instruments*, 2007, **78**, (1).

23 Ruan, J.-A., Bhushan, B.: 'Atomic-Scale Friction Measurements Using Friction Force Microscopy: Part I—General Principles and New Measurement Techniques' *J Tribol*, 1994, **116**, (2), pp. 378–388.

24 Di Paolo Emilio, M.: 'Data Acquisition Systems' (Springer New York, 2013)

25 Moreno, C., González, A., Olazagoitia, J.L., Vinolas, J.: 'The acquisition rate and soundness of a low-cost data acquisition system (LC-DAQ) for high frequency applications' *Sensors (Switzerland)*, 2020, **20**, (2).

26 Gao, S.H., Xue, B., Li, J., Lin, Z., Chen, Y., Zhu, X.Y.: 'High-resolution data acquisition technique in broadband seismic observation systems' *Sci China Technol Sci*, 2016, **59**, (6), pp. 961–972.

27 Chen, K., Chen, H., Huang, J., Lanni, F., Tang, S., Wu, W.: 'A Generic High Bandwidth Data Acquisition Card for Physics Experiments' *IEEE Trans Instrum Meas*, 2020, **69**, (7), pp. 4569–4577.

28 Fantner, G.E., Hegarty, P., Kindt, J.H., Schitter, G., Cidade, G.A.G., Hansma, P.K.: 'Data acquisition system for high speed atomic force microscopy' *Review of Scientific Instruments*, 2005, **76**, (2).

29 Jurgielewicz, P., Fiutowski, T., Kublik, E., *et al.*: 'Modular data acquisition system for recording activity and electrical stimulation of brain tissue using dedicated electronics' *Sensors*, 2021, **21**, (13).

30 Python TM, https://www.python.org/